IARJSET ISSN (O) 2393-8021, ISSN (P) 2394-1588

International Advanced Research Journal in Science, Engineering and Technology

Impact Factor 7.105 ⁜ Vol. 9, Issue 2, February 2022

DOI: 10.17148/IARJSET.2022.9219

Specific Absorption rate in ion doped $Y_3Fe_5O_{12}$ nanoparticles for self-controlling magnetic hyperthermia

A. T. Apostolov[1], I. N. Apostolova[2], J. M. Wesselinowa[3]

University of Architecture, Civil Engineering and Geodesy, Hristo Smirnenski Blvd.1, 1046 Sofia, Bulgaria[1]

University of Forestry, Kl. Ohridsky Blvd.10, 1756 Sofia, Bulgaria[2]

University of Sofia, J. Bouchier Blvd. 5, 1164 Sofia, Bulgaria[3]

Abstract: In this paper we study doped yttrium garnet (YIG) nanoparticles $Y_3\left[Fe_{2-y}M_y\right]_a(Fe_{3-z}M_z)_dO_{12}$, (M = Al, Ga, Sc are nonmagnetic ions), appropriate for Self-Controlled Magnetic Hyperthermia (SCMH) for in vivo and in vitro applications. A microscopic model (modified Heisenberg Hamiltonian) is presented, describing the super-exchange magnetic interactions in the tetrahedral and octahedral sublattices and between them. A methodology is proposed for determining the inter-sublattice and intra-sublattice exchange constants for different degrees of doping as well as the constants of single-ion magnetic anisotropy in dependence of temperature, concentration of doped magnetic ions and size of the magnetic nanoparticle (MNP). Using the Green's functions method, for the mixed yttrium garnet nanoparticles, the dependence of SAR coefficient on the amplitude and the frequency of the alternating magnetic dield, the temperature, and the magnetic inter-exchange interaction are studied. The calculations are made for monodisperse, non-interacting single-domain, heterogeneous spherical MNPs of the core/shell type.

Keywords: $Y_3Fe_5O_{12}$ nanoparticles; Magnetic properties; Ion doping; Green's function theory

I. INTRODUCTION

Magnetic hyperthermia (MH) is a comparatively new and innovative method for a fight of oncological diseases [1]. The numerous experiments demonstrate that the local heating of the tumours in the temperature range from 41° C to 46° C leads to their destruction and eventually to their complete disintegration while the healthy cells are preserved. This is due to the fact that tumours are more sensitive to overheating than healthy tissues.

The use of MNPs on biomedical applications has increased considerably in recent years. MNPs have been proposed as magnetic guidance in drug delivery and magnetic separation, as contrast agents in magnetic heat imaging, and as heat magnetic mediators in hyperthermia treatments [2-5]. The latter has been gaining lot of interest especially in the field of cancer treatment as an addition to other modalities such radiotherapy and chemotherapy.

MNPs-based hyperthermia has a number of advantages over conventional thermal heating for medical purposes: 1) MNPs can be directed through targeting agents to cancer formations, making the procedure selective; 2) Cancer cells absorb MNPs, thus generating heat only in the tissues associated with MNPs, i.e. the procedure is performed at the cellular level [6,7]. 3) MNPs are "clothed" in stable colloidal membranes and can be delivered to cancer formations in a non-invasive way: intravenously or intramuscularly.

In summary: the ideal mechanism for generating heat in tumour cells is non-invasive, preferably with precise localization; with high heating intensity and is temperature controllable.

Based on the above conditions, it is clear that it is extremely important to find methods for accurate monitoring of the heating temperature and for preventing overheating. It is not possible simply to turn off the magnetic field when the critical temperature is reached; at least due to the fact that the MNPs are not evenly distributed throughout the whole volume of the tumour and the temperature field is not homogeneous inside it. The solution of this problem is the use of MNPs (ferromagnetic or ferrimagnetic), which have a phase transition temperature T_C from a magnetically order ~~state~~ in magnetically disordered state in the range from 41° C to 46° C. Above this temperature, the particle goes into a paramagnetic state and the heating process stops, i.e. the process becomes self-regulating depending on the value of the temperature. This is called self-controlling magnetic hyperthermia. This means that the temperature of the magnetic phase transition can be considered as a necessary condition for a given MNP to be appropriate for the method of the SCMH, because it guarantees patient's safety. The additional conditions for MNPs to be applicable for SCMH are: a) High value of saturation magnetization M_S for greater response to the external magnetic field; b) Large value of the coercive field H_C, which leads to better efficiency of the thermal heating process; c) MNP size less than 35 nm, which allows possibility of their transportation through capillary blood vessels (for in vivo and in vitro application); d) Non-

IARJSET ISSN (O) 2393-8021, ISSN (P) 2394-1588

International Advanced Research Journal in Science, Engineering and Technology

Impact Factor 7.105 ⁜ Vol. 9, Issue 2, February 2022

DOI: 10.17148/IARJSET.2022.9219

toxicity and biocompatibility; e) The frequency f and the amplitude h_0 of the external alternating electromagnetic field must be biocompatible. High-frequency magnetic fields lead to involuntary excitation of peripheral and core muscles and nerves, cardiac stimulation and arrhythmia, as well as uncontrolled heating of tissues. This limit is defined by the expression: $h_0 * f < 6.2 \times 10^7$ Oe/s - called $h_0 * f$ factor [8].

An important condition for MNPs to be suitable for magnetic hyperthermia is their non-toxicity. This article will not examine toxicity issues in depth, but it will note a few key points. Improving the biocompatibility of MNPs is done by adding a special coat ("coating"). Examinations of MNPs coated with SiO_2 [9], dextran [10], cirtant ligands [11], fatty amino acids [12] and polyvinyl pyrrolidone [13] have shown colloidal stability and biocompatibility.

The use of MNPs for SCMH is connected with the dynamic response of the magnetic moment of the magnetic dipole in the alternating magnetic field and with the thermal fluctuations occurring in the MNPs. The mechanism of heat generation can be due to three phenomena: hysteresis losses, Neel's relaxation mechanism and Brownian's relaxation mechanism. The first mechanism is connected with the displacement of the domain walls and is observed in MNPs larger than a critical size by transition from a multi-domain to a single-domain phase [15]. For particles below the critical size and suitable for in vivo and in vitro application, the heating is due to the magnetic moment of the nanoparticle as a whole. In single-domain superparamagnetic particles, heat generation is due to the Neel-type relaxation mechanism [16] and the rotational Brownian-type relaxation mechanism [17]. In the Neel relaxation mechanism, the magnetic moments which are blocked in the direction of the easy axis of magnetization deviate from this axis in the direction of the external field. This mechanism is similar to the hysteresis losses in multidomain particles, as there is "internal friction" due to the rotation of the magnetic moments in the direction of the field, which leads to generation of heat. In the Brownian type, the whole particle oscillates with a magnetic moment in the direction of the easy axis, as the heat is being generated due to the viscous resistance of the medium. Neel and Brownian mechanisms act simultaneously, as the Brownian predominate for larger particles in low viscosity media [18], while Neel relaxation dominates for small particles and high viscosity biological solutions [16]. Which of the two mechanisms (hysteresis or relaxation) dominates depends on the volume of MNP. There is a critical volume of nanoparticles V_C [19], below which the relaxation predominates. Since the relaxation time τ_R of the MNP strongly depends on the particle size, it is proved that dominance occurs when τ_R is equal to the reciprocal value of the frequency of the alternating magnetic field f [20], i.e. $2\pi f \times \tau_R = 1$. For typical frequencies of the alternating magnetic fields used in SCMH ($f = 200$ kHz), the relaxation times of MNPs should be in the range of $10^{-5} \div 10^{-6}$ s, which according to [21] defines Neel relaxation as the dominant mechanism for single-domain nanoparticles with size below 35 nm (suitable for in vivo and in vitro applications).

To assess the efficiency of heat transfer from MNPs to tissues, the so-called SAR (specific absorption rate) coefficient is used, which is defined as the absorbed heat power normalized to the mass of the MNPs when an external alternating electromagnetic field with a gven frequency f and amplitude h_0 is applied:

$$\mathrm{SAR} = \frac{\text{Adsorbed power}}{\text{Mass of MNPs}} \quad (1)$$

If MNPs are placed in an alternating magnetic field with frequency f and amplitude h_0, the heat A will be released in one cycle of the alternating magnetic field equal to the area of the hysteresis curve. The SAR per unit mass of the infiltrated MNP's sample is then defined as:

$$\mathrm{SAR} = \mathrm{Af}. \quad (2)$$

The quantitative characterization of the efficiency of transformation of magnetic energy into heat is determined by the possibility to calculate the area of the hysteresis curve and the dependence of this area on the parameters characterizing the properties of MNP.

For the treatment of tumors by SCMH, three groups of compounds have been examined thoroughly: Single-domain magnetites (Fe_3O_4 or γ-Fe_3O_4), which have excellent biocompatibility[22], iron oxides of structural formula $Me_{1-x}Zn_xFe_2O_4$, where Me = Ni, Co, Mn, Zn, Mg,[23,24], Sr-ion doping of manganese perovskite with the structural formula $La_{1-x}Sr_xMnO_3$.[25,26] and yttrium garnets doped with trivalent diamagnetic Al^{3+}, Sc^{3+}, In^{3+} and Ga^{3+} ions with structure formula $Y_3\left[Fe_{2-y}M_y\right]_a(Fe_{3-z}M_z)_dO_{12}$[27-29].

In our previous studies,[23,25,29] modelling the heterogeneity in single-phase nanoparticles with a change in the exchange interaction constants, magnetic anisotropy and number of nearest neighbours in the surface and in the core, we investigated in detail MNPs for the last three groups and determined MNPs, which are suitable for SCMH based on their magnetic phase transitions, size, magnetization and coercivity values.

In our paper [29] we study doped yttrium garnet (YIG) nanoparticles $Y_3\left[Fe_{2-y}M_y\right]_a(Fe_{3-z}M_z)_dO_{12}$, (M = Al, Ga, Sc are nonmagnetic ions), appropriate for Self-Controlled Magnetic Hyperthermia (SCMH) for in vivo and in vitro applications. We theoreticaly find a set of mixed yttrium garnet magnetic nanoparticles (NPs), which are suitable for

IARJSET ISSN (O) 2393-8021, ISSN (P) 2394-1588

International Advanced Research Journal in Science, Engineering and Technology

Impact Factor 7.105 ⁜ Vol. 9, Issue 2, February 2022

DOI: 10.17148/IARJSET.2022.9219

applications in medicine for cancer therapy. There are two Sc doped YIG NPs which are the best candidates for SCMH with x = 1.08, d = 27.5 nm, SAR_{max} = 13.52 $W.g^{-1}$ as well as x = 1.10, d = 29.7 nm, SAR_{max} = 15.44 $W.g^{-1}$ for which the conditions for bio-compatibility and maximization of SAR are fulfilled simultaneously. Moreover, we have found also Al and Ga doped YIG NPs which can be applied for the magnetic hyperthermia but with something smaller SAR effectivity[29].

YAlG			YGaG			YScG		
x	d (nm)	SAR(W/g)	x	d (nm)	SAR(W/g)	x	d (nm)	SAR(W/g)
1.67	26.0	4.26	1.62	26.0	4.78	1.06	24.0	5.18
1.71	28.0	7.34	1.65	31.8	12.05	1.08	26.0	8.13
1.75	33.8	13.94				1.10	33.0	4.18

Table 1 SAR values for YAlG, YGaG and YScG for particles with diameter applicable for in vivo and in vitro therapy and with a bio-acceptable temperature of the phase transition of T = 315 K[29].

But the SAR values depend also for external parameters - the amplitude of the alternating magnetic field h_0 and its frequency f, as well as microscopic parameters – magnetic exchange interactions, magnetic anisotropy.
The aim of the present paper, on the basis of entirely microscopic mechanism proposed by us [30] for calculating the SAR, to study the dependence of the thermal efficiency for (YIG) nanoparticles $Y_3[Fe_{2-y}M_y]_a(Fe_{3-z}M_z)_dO_{12}$, (M = Al, Ga, Sc are nonmagnetic ions) on the characteristics of the alternating magnetic field and the magnetic exchange interactions. This requires the calculation of the dynamic characteristics of the systems: energy of spin excitations, their damping and the relaxation time, giving the response of the magnetic system to an external alternating magnetic field.

II. MODEL AND METHOD

The compound yttrium iron garnet has a cubic structure with a space group of symmetry $O_h^{10} - Ia3d$ [31]. The location of Fe^{3+} and Y^{3+} ions are shown on Fig. 1.

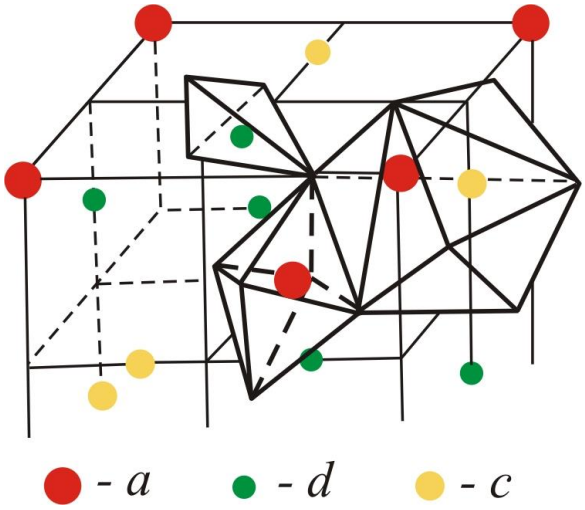

Fig. 1 Octahedral (a-sites), tetrahedral (d-sites) and dodecahedral (c-sites) sites in the unit cell of the yttrium iron garnet.

The distribution of the cations in the garnet's lattice depends on their size as the Y^{3+} ions having the largest diameter occupy the c-sites, while the a-sites and d-sites have been occupied by the smaller Fe^{3+} ions. Since yttrium ions are nonmagnetic, there are only two magnetic sublattices formed by iron ions at the 16a and 24d places, which are situated antiferromagnetically relative to each other [32]. The ratio of tetrahedral (d-places) and octahedral (a-places) sites is 3 to 2. Thus the net magnetic moment is in the direction of the magnetization of the d-sublattice. The appearance of ferrimagnetic arrangement and magnetic phase transition below T_N = 599 K [33] is due to the inter-sublattice super-exchange interaction J^{ad} between magnetic Fe^{3+} ions in tetrahedral and octahedral sites mediated by oxygen ion which is the strongest magnetic exchange interaction in this system. The intra-sublattice interactions J^{aa} and J^{dd} are small due to the unfavourable location of the ions in the sublattices [34].

IARJSET ISSN (O) 2393-8021, ISSN (P) 2394-1588

International Advanced Research Journal in Science, Engineering and Technology

Impact Factor 7.105 ⁜ Vol. 9, Issue 2, February 2022

DOI: 10.17148/IARJSET.2022.9219

Substitution of Fe^{3+} ions with nonmagnetic ions (e. g. Al^{3+}, Ga^{3+}, Sc^{3+}, In^{3+}) leads to a change in the magnetization of the doped YIG samples. This is associated with a change in the number of magnetic ions in the tetrahedral and octahedral sites, as the magnetic moment will increase with the replacement of Fe^{3+} ions at the a-places with Sc^{3+}, In^{3+} ions and will decrease with replacement the iron at d-places with Al^{3+}, Ga^{3+} ions. In both cases, this will reduce the Curie temperature T_C compared to the undoped sample because the number of magnetic interactions per formula unit decreases [31,32,35,36]. Thus the formula of mixed garnets has the form: $Y_3\left[Fe_{2-y}M_y\right]_a(Fe_{3-z}M_z)_dO_{12}$ where y and z determine the part of the nonmagnetic ions occupying the octahedral and tetrahedral places, respectively, as $x = y + z$ determines the degree of doping.

The Hamiltonian which will describe the magnetic characteristics of mixed garnets with structural formula $Y_3\left[Fe_{2-y}M_y\right]_a(Fe_{3-z}M_z)_dO_{12}$ has the form:

$$H(x) = -\sum_{<ik>} J_{ik}^{ad}(x)\left(\vec{S}_i^a.\vec{S}_k^d\right) - \sum_{<lj>} J_{lj}^{da}(x)\left(\vec{S}_l^d.\vec{S}_j^a\right) - \sum_{<ij>} J_{ij}^{aa}(x)\left(\vec{S}_i^a.\vec{S}_j^d\right)$$
$$-\sum_{<kl>} J_{kl}^{dd}(x)\left(\vec{S}_k^d.\vec{S}_l^d\right) - \sum_i K_{1i}^a(S_i^{az})^2 - \sum_i K_{1i}^d\left(S_i^{dz}\right)^2 - g\mu_B\sum_i \vec{h}.\left(\vec{S}_i^a + \vec{S}_i^d\right), \quad (3)$$

where $\vec{S}_i^\gamma$ for $\gamma = a, d$ is the Heisenberg spin operator in the γ-sublattice at the i-crystallographic place. The first two terms define the exchange interactions between a- and d- sublattices. Although the super-exchange inter-sublattice interactions J^{ad} and J^{da} are equal, the first two terms are separated due to the fact that the first neighbours in the interaction of a magnetic ion from the a-sublattice with the magnetic ions from the d-sublattice ($< ad >^0 = 6$) are different from the number of the nearest neighbours in the interaction of a magnetic ion from the d-sublattice with the magnetic ions from the a-sublattice ($< da >^0 = 4$). For completeness, we note that the number of nearest neighbours in internal sublattice interactions is $< aa >^0 = 6$ and $< dd >^0 = 4$ for a- and d- sublattices, respectively. In mixed garnets, when the number of nonmagnetic ions changes in consequence of substitution, we have a direct decrease in the number of interacting nearest neighbours in a- and d- sublattices and between them. The reduction of the nearest neighbours will of course depend on the degree of doping x and how the nonmagnetic ions are distributed (preferentially) on the tetrahedral and octahedral sites and can be expressed as follows:

$$< ad >=< ad >^0\left(1-\frac{z}{3}\right);\quad < da >=< da >^0\left(1-\frac{y}{2}\right);$$
$$< dd >=< dd >^0\left(1-\frac{z}{3}\right);\quad < aa >=< aa >^0\left(1-\frac{y}{2}\right). \quad (4)$$

The third and fourth terms in eq. (3) define the intra-sublattice super-exchange interactions J^{aa} and J^{dd}. As noted above, these two interactions are antiferromagnetic and are an order of magnitude smaller than the inter-sublattice, i.e. the following inequation is valid: $\left|J^{ad}\right| \gg \left|J^{dd}\right| > |J^{aa}|$. K^γ for $\gamma = a, d$ determines the value of the single-ion anisotropy of the magnetic ions in the octahedral and tetrahedral sites, $\vec{h}$ is the external magnetic field.

For small MNPs (appropriate for in vivo and in vitro application with size up to 35 nm) their heterogeneity should be taken into account because the altered surface properties with respect to bulk samples significantly affect the magnetization, coercivity and temperature of the magnetic phase transition. We consider the nanoparticle divided into two parts a core and a surface shell. The surface of the MNP consists of spins with a reduced number of neighbours due to broken periodic invariance, unpaired electronic orbitals, oxidation and vacations. From a microscopical point of view, we shall model a heterogeneous MNP of the core/shell type by defining different interaction constants and magnetic anisotropy in the surface layer and core. With the index "s" we denote all characteristics and interactions in the shell, and with the index "b" - all characteristics and interactions in the core. The interruption of the $Fe^\gamma - O - Fe^\gamma$ bonds on the surface lead to an increase in the ionic character and will probably lead to an increase of the lattice constant of the shell compared to the bulk samples. This reduces the magnitude of the super-exchange interaction J^{ad} and an antiferromagnetic arrangement in the surface layer or spin disorder surface layer [37,38] is appeared. Thus, the model of the magnetically “dead” surface layer can be used. Our model allows, taking into account that $J_s^{ad} < J_b^{ad}$, and also the competition between the ferrimagnetic and antiferromagnetic arrangements, to modulate a noncollinear spin arrangement of the surface. Such a noncollinear spin arrangement of the YIG nanoparticle surface has been reported in [39]. Experimental studies have shown that the magnetic anisotropy in bulk samples of YIG’s is a two order of magnitude smaller than that in MNPs [40,41]. We assume that there is no interaction between the individual particles and the probe is homogeneous, i.e. all particles are spherical with the same size.

Instead of the spin operators $\left(S_i^\gamma\right)^x$ and $\left(S_i^\gamma\right)^y$ we enter the following operators:

$$\left(S_i^\gamma\right)^\pm = \left(S_i^\gamma\right)^x \pm \left(S_i^\gamma\right)^y.$$

IARJSET ISSN (O) 2393-8021, ISSN (P) 2394-1588

International Advanced Research Journal in Science, Engineering and Technology

Impact Factor 7.105 ⁜ Vol. 9, Issue 2, February 2022

DOI: 10.17148/IARJSET.2022.9219

To calculate the magnetic characteristics of mixed garnet's MNPs, we use the Green's functions (GFs) method which finds wide application in the study of multiparticle complex systems, whose separate subsystems are intensively influenced. This leads to an appearance of nonlinear interactions, in which a small parameter is missing and the application of the standard perturbations methods are not applicable. GFs are universal approach to calculating the static and dynamic characteristics of different systems. The formalism is very convenient because it does not consider operators, but rather complex functions that have simple analytical properties. The GF allows a uniform solution to all quantum statistical problems of multiparticle systems without the need to develop separate methods. Taking into account the broken translational invariance responsible for the occurrence of surface and size effects the exchange interaction constants can have different values on the surface and in the bulk [42]. The observed analytical expressions are numericaly calculated in order to study the temperature dependences of static and dynamic properties.
We define the following retarded GFs:

$$\begin{aligned} G_{ij,E}^{ad} &= \ll S_i^{a+};\ S_j^{d-} \gg_E; \\ G_{ij,E}^{da} &= \ll S_i^{d+};\ S_j^{a-} \gg_E; \\ G_{ij,E}^{aa} &= \ll S_i^{a+};\ S_j^{a-} \gg_E; \\ G_{ij,E}^{dd} &= \ll S_i^{d+};\ S_j^{d-} \gg_E. \end{aligned} \tag{5}$$

Using the equation of motion:

$$EG_{ij} = \frac{i}{2\pi} < \left[S_i^{+};\ S_j^{-}\right] > + \ll \left[[S_i^{+}; H];\ S_j^{-}\right] \gg. \tag{6}$$

We have calculated the GFs in the random phase approximation (RPA), eq. (A.1) which is given in Appendix A.
The magnetization of the system is:

$$M_S(T) = |(3-z)C_d(y)M_{sd}(T) - (2-y)C_a(z)M_{sa}(T)|, \tag{7}$$

where the functions $C_d(y)$ and $C_a(z)$ are determined empirically by modifying the Neel's model of ferrimagnetism. They are calculated taking into account the random distribution of nonmagnetic ions around magnetic Fe^{3+} ions in tetrahedral and octahedral sites and taking into account the fact that nonmagnetic ions in one sublattice affect the interaction in the other sublattice [43]. In the framework of the present work, we use the explicit nature of these functions defined by Roschmann et al. [44] as follows:

$$\begin{aligned} &C_a(z) = 1 - \alpha\left(\frac{z}{3}\right)^6 \text{ as } \alpha(Ga) = 2.2 \text{ and } \alpha(Al) = 1.6; \\ &C_d(z) = 1 - 70.02y - 2\left(\frac{y}{2}\right)^4 \text{ for Al; Sc; Ga; In,} \end{aligned} \tag{8}$$

where the index α is introduced in order to fit better the experimental data by doping with different nonmagnetic ions.
The magnetization of a- and d- sublattices is calculated to:

$$M_{s\gamma} = \frac{1}{N_\gamma}\sum_k < S_k^{\gamma z} >;\ \gamma = a; d. \tag{9}$$

$< S_k^{\gamma z} >$ is determinated by the following equation [45]:

$$< S_k^{\gamma z} >= (S^\gamma + 0.5)\coth\left[(S^\gamma + 0.5)\beta\xi_k^\gamma\right] - 0.5\coth\left[0.5\beta\xi_k^\gamma\right], \tag{10}$$

where $\beta = \frac{1}{k_B T}$ and $\xi_k^\gamma = \frac{1}{N_\gamma}\sum_l \xi_{kl}^\gamma;\ \gamma = a; d.$

The expressions of the energies ξ_{kl}^γ are given in Appendix B. In order to calculate the ξ_{kl}^γ beyond the RPA the following correlation functions must be defined: $< S_i^{d-}S_j^{a+} >$; $< S_i^{a-}S_j^{d+} >$; $< S_i^{a-}S_j^{a+} >$ and $< S_i^{d-}S_j^{d+} >$. Using the spectral theorem [46] we get:

$$\begin{aligned} &< S_i^{a-}S_j^{a+} >= \frac{1}{2\pi}\left\{\Phi^{aa}\left(E_{ij}^1\right) + \Phi^{aa}\left(E_{ij}^2\right)\right\} < S_i^{az} > \delta_{ij}; \\ &< S_i^{d-}S_j^{d+} >= \frac{1}{2\pi}\left\{\Phi^{dd}\left(E_{ij}^1\right) + \Phi^{dd}\left(E_{ij}^2\right)\right\} < S_i^{az} > \delta_{ij}; \\ &< S_i^{a-}S_j^{d+} >= -< S_i^{d-}S_j^{a+} >= \frac{J_{ij}^{ad}}{\pi}\left\{\Theta\left(E_{ij}^1\right) + \Theta\left(E_{ij}^2\right)\right\} < S_i^{az} >< S_j^{dz} >, \end{aligned} \tag{11}$$

IARJSET ISSN (O) 2393-8021, ISSN (P) 2394-1588

International Advanced Research Journal in Science, Engineering and Technology

Impact Factor 7.105 ⁜ Vol. 9, Issue 2, February 2022

DOI: 10.17148/IARJSET.2022.9219

where:

$\Phi^{\gamma\gamma}(E)\frac{=(2-\Psi_{ij})(E-E_{ij}^{\gamma\gamma})}{\exp\left(\frac{E}{k_B T}\right)-1}$, $\gamma = a, d$; $\Theta(E) = 2E - \Psi_{ij}$ and $\Psi_{ij} = E_{ij}^{aa} + E_{ij}^{dd}$.

$E_{ij}^{1,2}$ is the excitation energy between two local spins in the sites i and j determined self-consistently by the poles of the GFs (eq. (A.1)).

$$E_{ij}^{1,2} = 0.5\left(E_{ij}^{aa} + E_{ij}^{dd}\right) \pm \left[\left(E_{ij}^{aa} - E_{ij}^{dd}\right)^2 - 4E_{ij}^{ad}E_{ij}^{da}\right]^2. \quad (12)$$

Most theories for calculating SAR are macroscopic: based on Debye's description of dielectric losses, which leads to the creation of the so-called linear response theory (LRT) [16,47]; based on the Stoner-Wohlfarth model in the numerical calculation of the Landau-Lifshitz equation with simulations through the Monte-Carlo method [14,48,49]. All these models are characterized by intuitiveness and interpretability of individual aspects of this complex task. They have been constantly modified and supplemented in order to improve the understanding of the mechanisms of magnetic hyperthermia and to improve the predictions of these theories [50-53]. An entirely microscopic model for calculating SAR was recently proposed by Apostolova et al. [30], which makes it possible to study thermal efficiency as a function of the microscopic magnetic characteristics of the system and the energy of elementary excitations and damping. Briefly, in our study, based on Kubo formalism, the average absorbed power P of the MNP has been calculated for the first time, finding the imaginary part of the magnetic susceptibility $\chi''_{pq}(\omega)$

$$P = -2\sum_{\substack{p,q \\ \omega>0}} \omega\chi''_{pq}(\omega)h^p_{max}\,h^q_{max}, \qquad p, q = x, y, z, \quad (13)$$

where $\chi''_{pq}(\omega)$ is the imaginary part of the magnetic susceptibility and on microscopic level is expressed by a retarding Green's function. For antiferromagnetic and ferrimagnetic nanoparticles the magnetic susceptibility has the form:

$$\chi_{pq}(\omega) = -\sum_{\substack{ij \\ \gamma,\eta}} g^2\,\mu_B^2\,\langle\langle\left(\vec{S}_i^{\gamma}\right)^p;\left(\vec{S}_j^{\eta}\right)^q\rangle\rangle_{\omega}, \quad (14)$$

where $\gamma, \eta = a, d$ are the spin variables in the defined sublattices, i, j determine the summation by the nearest neighbours, $\omega = 2\pi f$, g is the gyromagnetic ratio and μ_B is the Bohr magneton. From eq. (14) the area of the hysteresis curve can be calculated through quantities characterizing the system from a microscopic point of view. This gives us the opportunity, on the basis of a properly defined model Hamiltonian, to calculate the necessary Green's functions $\langle\langle\left(\vec{S}_i^{\gamma}\right)^p;\left(\vec{S}_j^{\eta}\right)^q\rangle\rangle_{\omega}$ using the method of Tserkovnikov [54]. From the expression $SAR = \frac{Pf}{\rho}$ we are able to determine the dependences of the thermal heating efficiency on the microscopic characteristics of the magnetic system.

To calculate the SAR we must include the damping effects. Without limiting the community we will assume that the Green's functions have poles in the lower part of the complex plane, i.e. $\widetilde{E}_{ij} = \pm E_{ij} - i\gamma_{ij}$. E_{ij} and γ_{ij} are the energy of the spin excitations shown in eq. (12) and the damping, respectively. For the calculation of the latter we use the following expression:

$$\Gamma_{ij} = \lim_{t\to\infty} \mathrm{Im}\left\{\frac{i}{t}\int dt' t' \left[\frac{\langle j_i(t); j_j^+(t')\rangle}{\langle S_i^+(t); S_j^-(t')\rangle}\right]\right\}, \quad (15)$$

where $j_i(t) = \langle[S_i^+, H]\rangle$.

In order to find the absorbed power P we must calculate the inter- and intra-sublattices spin damping $\Gamma_{ij}^{\gamma\eta}$. The equations of the damping are given in Appendix C and are calculated from eq. (15).

If a linearly polarized magnetic field is attached to the x–axis, in order to obtain the analytical expression for the absorbed power P, we must calculate the transverse susceptibility $\chi^{xx}(\chi_{\perp})$. Without going into details by following our calculations in [30] for the average absorbed power P we get:

$$P = 4\sum_{ij}\frac{2g^2\mu_B^2}{\pi} * \frac{EA_2}{E^2+A_1} * \Gamma_{tot} * \left[\frac{\left\{\left[E-E_{ij}^{dd}+2E_{ij}^{da}\right]\langle S_l^{az}\rangle\right\}}{[\Lambda(E)]^2+4E^2(\Gamma_{tot})^2} + \frac{\left\{\left[E-E_{ij}^{aa}+2E_{ij}^{ad}\right]\langle S_l^{dz}\rangle\right\}}{[\Lambda(E)]^2+4E^2(\Gamma_{tot})^2}\right] E^2(h_0)^2, \quad (16)$$

where: $\Lambda(E) = \frac{\left(E^2-A_1\right)^2-E^2A_2^2-E^2(\Gamma')^2+A_3^2}{E^2+A_1}$, $\Gamma_{tot} = \Gamma' + \frac{A_2A_3}{E^2+A_1}$, and the terms for A_1, A_2, A_3, Γ' are given in Appendix C.

IARJSET ISSN (O) 2393-8021, ISSN (P) 2394-1588

International Advanced Research Journal in Science, Engineering and Technology

Impact Factor 7.105 ⁜ Vol. 9, Issue 2, February 2022

DOI: 10.17148/IARJSET.2022.9219

For garnet (YIG) nanoparticles $Y_3\left[Fe_{2-y}M_y\right]_a(Fe_{3-z}M_z)_dO_{12}$, (M = Al, Ga, Sc are nonmagnetic ions), appropriate for Self-Controlled Magnetic Hyperthermia (SCMH) for in vivo and in vitro applications determined in [29] we study the dependence of the thermal efficiency for dopped nanoparticles on the characteristics of the alternating magnetic field and the magnetic exchange interactions.

III. NUMERICAL RESULTS AND DISCUSSION

Now we present the numerical calculations for the SAR values as a function of parameters of the alternating magnetic field for mixed garnet nanoparticles with structural formula $Y_3\left[Fe_{2-y}M_y\right]_a(Fe_{3-z}M_z)_dO_{12}$, where M = Al, Ga, Sc. From the above discussion it is clear that from a magnetic point of view the MNPs are single-domain, heterogeneous of the core/shell type, the probe is monodisperse and there is no interaction between the particles. A homogeneous distribution of MNPs in the heating region is assumed. We consider that the doping does not change the type of the elementary cell. The difference in the sizes of the magnetic Fe ions and the substitution with nonmagnetic ions change the number and intensity of spin's interaction in the sublattices and between them.

For numerical calculations, the values of the super-exchange magnetic interactions (intra- and inter- sublattice) must be determined depending on the degree of x with nonmagnetic ions. As already noted, nonmagnetic ions can occupy both octahedral and tetrahedral places. The distribution of doped ions at the a- and d- sites can be determined experimentally by nuclear-magnetic resonance imaging [55] or on the basis of thermodynamic calculations of two energies equilibrium cation distribution model [32,56]. The values of J^{ad}, J^{aa} and J^{dd} are determined from their relationship with the molecular field coefficients N_{ad}, N_{aa} and N_{dd} using the following expression [31]:

$$J^{\gamma\eta} = B\frac{n_\eta}{<\gamma\eta>}N_{\gamma\eta}, \tag{17}$$

where: $\gamma, \eta = a, d$ and $B = \frac{1}{16}g_\gamma g_\eta \mu_B^2 a^3 N_A$ with the following notations: n_η - the number of Fe ions in the γ sublattice, $N_{\gamma\eta}$ - the molecular field coefficients, $< \gamma\eta >$ - the number of the nearest neighbours for a given magnetic ion in the γ sublattice, g_η - the factor of spectroscopic splitting, μ_B - the Bohr magneton, a - the crystal lattice constant, and N_A - the Avogadro constant.

Based on experimental data for magnetization as a function of temperature and using Neel's phenomenological theory of molecular field (TMF) for ferromagnetism, Anderson determines the molecular field coefficients (MFC) for undoped YIG [57]. Dionne [43] observed a set of expressions determining the dependence of $N_{\gamma\eta}$ on the doping concentration of nonmagnetic ions by modifying the TMF for doped yttrium garnet and using data for $M_S(T)$. He performs this under the following assumptions: 1) The replacement of magnetic ions with nonmagnetic ions in d-sublattice is the reason for the decrease of the value of N_{aa} without changing the value of N_{dd} and vice versa; 2) N_{ad} decreases depending on the statistical distribution of the nonmagnetic ions in both sublattices. The following relation is valid:

$$N_{\gamma\eta}(y,z) = F_{\gamma\eta}(y,z)N_{\gamma\eta}(0,0), \tag{18}$$

where $F_{\gamma\eta}(y,z)$ is a dilution function.

Roschmann et al. [56] based on the analysis of the temperature dependence of the saturation magnetization for different nonmagnetic doping ions (Al, Ga, Sc) derive a system of $F_{\gamma\eta}(y,z)$ functions:

$$\begin{aligned} F_{ad}(y,z) &= 1 - f(y+z) - b(y-3z)^2; \\ F_{aa}(y,z) &= (1-\tfrac{z}{3})(1 - cz + gz^2); \\ F_{dd}(y,z) &= (1-\tfrac{y}{2})(1+ey)^2, \end{aligned} \tag{19}$$

as for the set of values the molecular field coefficients for undoped YIG we use those obtained in [56]:

$$N_{ad} = 98\,\frac{mole}{cm^3};\ N_{dd} = -67.8\,\frac{mole}{cm^3};\ N_{aa} = -30.4\,\frac{mole}{cm^3}. \tag{20}$$

IARJSET ISSN (O) 2393-8021, ISSN (P) 2394-1588

International Advanced Research Journal in Science, Engineering and Technology

Impact Factor 7.105 ⁜ Vol. 9, Issue 2, February 2022

DOI: 10.17148/IARJSET.2022.9219

For the coefficients f, b, c, g, e from eq. (19) the following values were observed:

Dopant	f	b	c	g	e
Al	0.12	0.011	0.18	0.01	0.06
Ga	0.14	0.124	0.19	0.01	0.07
Sc	0.123	0.013	0.2	0.01	0.07

Table2 Coefficients for the dilution functions of eq. (19) according to [56].

Substituting eq. (18) into eq. (17) we obtain:

$$J^{\gamma\eta}(y,z) = \left[\frac{a(y,z)}{a(0,0)}\right]^3 \frac{n_\eta <\gamma\eta>^o}{<\gamma\eta> n_\eta{}^o} F_{\gamma\eta}(y,z) J^{\gamma\eta}(0,0) = F_{\gamma\eta}(y,z) \left[\frac{a(y,z)}{a(0,0)}\right]^3 J^{\gamma\eta}(0,0), \quad (21)$$

where $<\gamma\eta>^o$ and $n_\eta{}^o$ determine the number of the nearest neighbours of a given magnetic ion in inter- and intra-sublattice interactions and the number of magnetic ions in the γ- sublattice for undoped YIG. Taking into consideration that $n_d = 3 - z$ and $n_a = 2 - y$ calculating $F_{\gamma\eta}(y,z)$ for given y and z at known values of $J^{\gamma\eta}(0,0)$ for undoped YIG we determine the values of the exchange magnetic interaction between tetrahedral and octahedral places as well as for each magnetic sublattice for different doping of nonmagnetic ions. For completeness it should be noted that as the number of nonmagnetic ions increases, the constant of the crystal lattice changes, which requires in eq. (21) to add a term of the form $\left[\frac{a(y,z)}{a(0,0)}\right]^3$ (see in eq. (17) the constant $B = \frac{1}{16} g_\gamma g_\eta \mu_B^2 a^3 N_A$). This term, for example, by doping with Al ions for values of x in the range from 0 to 1.75 varies in the range $1 \div 0.967$ [58] and defines an error in the range from 0 to 3.3 %, which can be ignored. From the implemented analysis, the type of expression by which we will calculate $J^{\gamma\eta}(y,z)$ has the form:

$$J^{\gamma\eta}(y,z) = F_{\gamma\eta}(y,z) J^{\gamma\eta}(0,0) \quad (22)$$

For super-exchange interaction constants $J^{\gamma\eta}(0,0)$ of undoped YIG we will use those published in [58]: $J^{ad} = -36.84$ K, $J^{dd} = -2.59$ K and $J^{aa} = -1.30$ K. Using eq. (21) and eq. (22) the values $J^{\gamma\eta}(y,z)$ for YIG doped with Al, Ga, Sc and In are numericaly calculated and presented in Fig 2. Distribution of the nonmagnetic ions x in the octahedral y and tetrahedral z sites in the mixed yttrium garnet $Y_3\left[Fe_{2-y}Al_y\right]_a(Fe_{3-z}Al_z)_dO_{12}$ used for the the calculated super-exchange inter- and intra- sublattice interactions are taken from papers as follows: 1/ for Al^{3+} [35,36,44]; 2/ for Ga^{3+} [36,44]; 3/ for Sc^{3+} [32,59] and 4/for In^{3+} [31,32].

However, indium is incompatible with biological matter, making it impossible to use the compounds $Y_3\left[Fe_{2-y}In_y\right]_a(Fe_{3-z}In_z)_dO_{12}$ for in vivo and in vitro medical applications. Its compounds are toxic when injected into the blood. They damage the heart, kidneys and liver. Its inclusion is for the purpose of completeness of the exposition and comparative analysis with results obtained with mixed yttrium garnet doped with Sc (for more information see [29]).

The magnetic anisotropy, which we use in the numerical calculations, depends on the temperature, the degree of doping with nonmagnetic ions and the size of the nanoparticles. The values of K_1 are presented graphically in Fig. 3 a) and Fig. 3 b) determining the dependence of the first constant of magnetic anisotropy on the concentration of nonmagnetic ions Ga^{3+} (curve 1) and In^{3+} (curve 2) for two values of temperature $T = 5$ K Fig. 3 a) and room temperature ($T = 300$ K) Fig. 3 b). The curves are constructed on the basis of experimental data published in [59-63].

For completeness, we note that for YIG for all temperatures the values of K_1 are negative. This means that the axes of the easy magnetization are along the body diagonal of the cube, while the axes of the hard magnetization are along the edge of the cube. In the mixed garnets, examined by us, only Fe^{3+} ions are magnetic, and it can be concluded that the dependence of the constant of the single-ion magnetic anisotropy on x will have the same character as presented in Fig. 3 a) and Fig. 3 b), regardless of the type of the doping ion. Of course, the values of K_1 will depend on the size of the doping ion, which, depending on its radius, will cause compressive or tensile strain of the lattice and change of the internal crystal field. Moreover, within the single-ion model, the anisotropy is considered to be an additive characteristic of the individual ions, depending only on the type of magnetic ion and the crystallographic

IARJSET ISSN (O) 2393-8021, ISSN (P) 2394-1588

International Advanced Research Journal in Science, Engineering and Technology

Impact Factor 7.105 ⁜ Vol. 9, Issue 2, February 2022

DOI: 10.17148/IARJSET.2022.9219

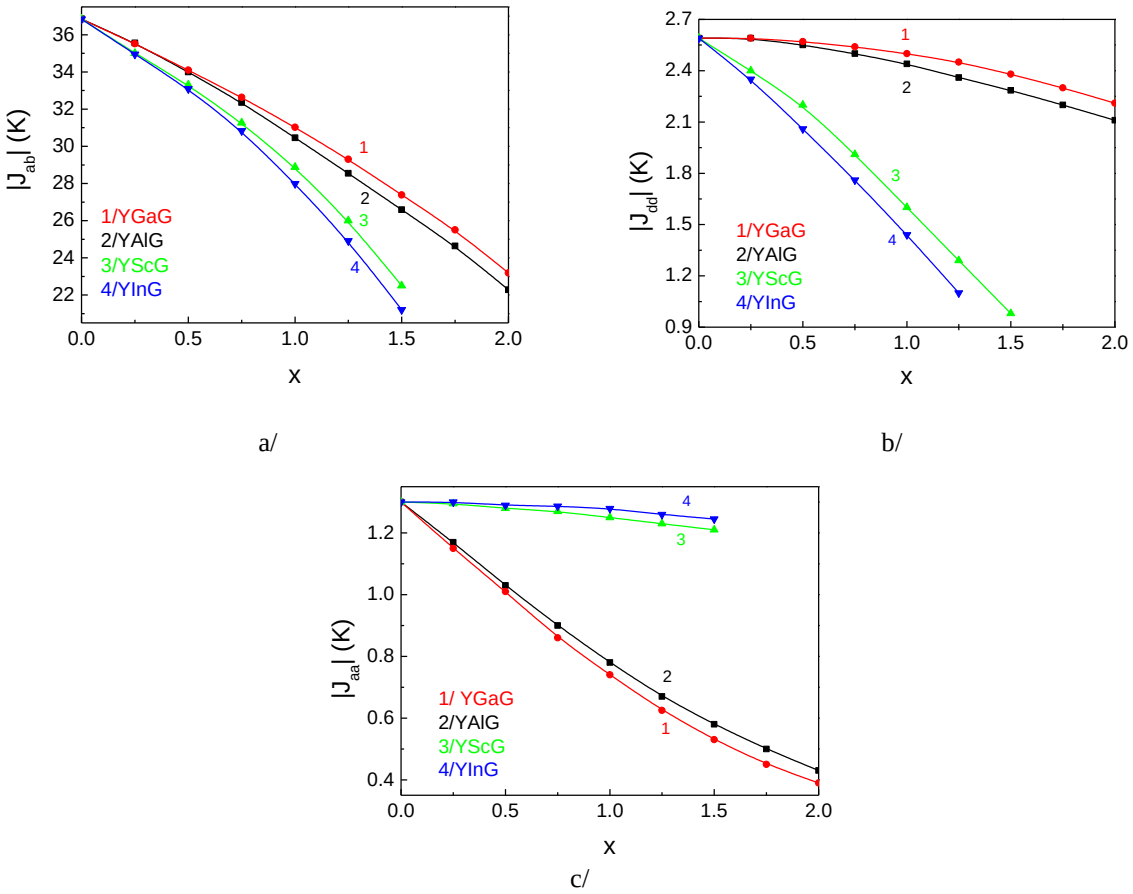

Fig. 2 Dependence of the constant of a/ inter-super-exchange interaction $|J_{ad}|$ b/ intra- sublattice interaction between tetrahedral d-sites $|J_{dd}|$ and c/ intra-sublattice interaction between octahedral a-sites $|J_{aa}|$ on the degree of doped with nonmagnetic ions: 1/ Al^{3+} curve 1 2/ Ga^{3+} curve 2; 3/ Sc^{3+} curve 3 and 4/ In^{3+} curve 4.

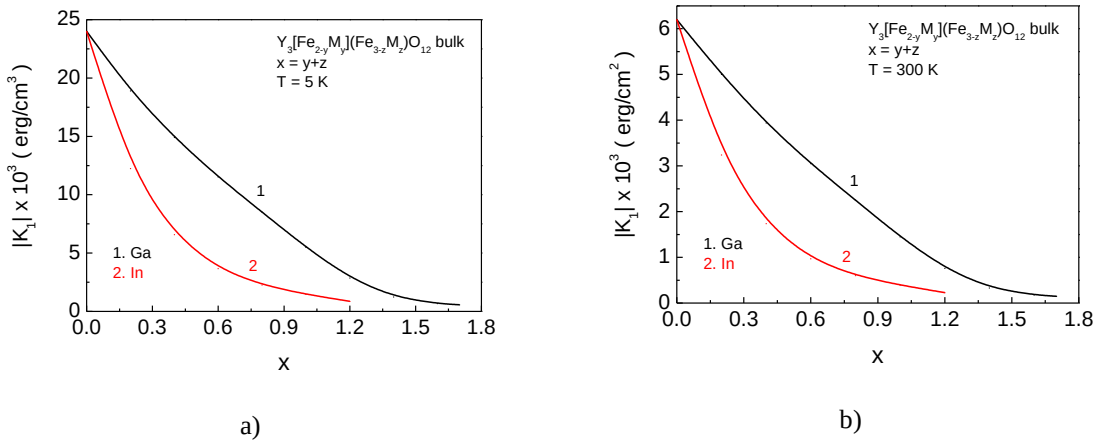

Fig. 3 Dependence of the constant of magnetic anisotropy $|K_1|$ on the degree of doped with nonmagnetic ions: Ga^{3+} curve 1 and In^{3+} curve 2 for different values of temperature a) $T = 5$ K and b) $T = 300$ K.

position occupied by it. Because of this reason, we assume that when doping with nonmagnetic ions with a radius smaller than that of Fe^{3+} (Al, Ga) the dependence of K_1 on x is determined by curve 1 in Fig. 3 a) and Fig. 3 b), and when doping with an ion with more large radius (In, Sc) curve 2 of the same figures.

IARJSET ISSN (O) 2393-8021, ISSN (P) 2394-1588

International Advanced Research Journal in Science, Engineering and Technology

Impact Factor 7.105 ⁜ Vol. 9, Issue 2, February 2022

DOI: 10.17148/IARJSET.2022.9219

In the calculations we use the temperature dependence of the YIG constant on an undoped bulk sample. This dependence is depicted in Fig. 4 a) and is constructed on the basis of experimental data published in [64]. We shall consider that the temperature dependence does not change at a given value of the degree of doping x.

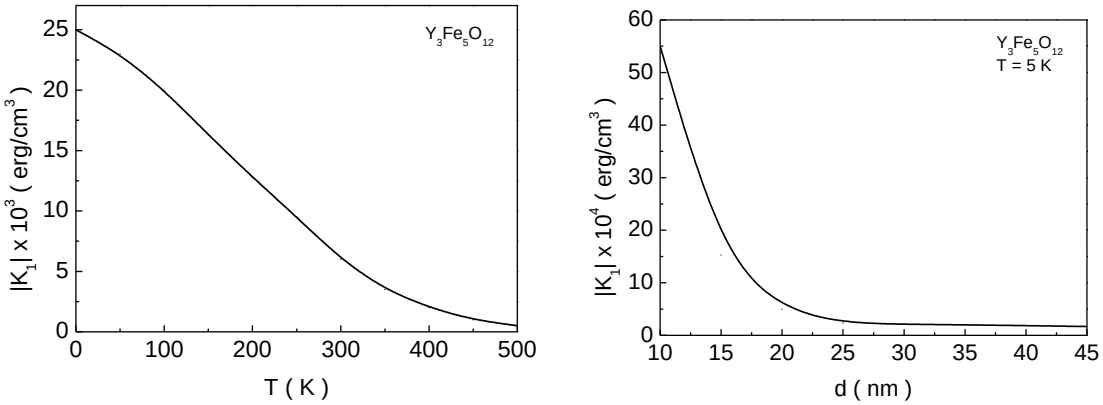

a) b)

Fig. 4 The dependence of the magnetic anisotropy constant $|K_1|$ on: a) the temperature T and b) the size d of the nanoparticles at $T = 5$ K for undoped YIG.

The additivity of the single-ion anisotropy allows to calculate for each value of x and T the constant K_1 for one magnetic ion for a given mixed garnet in Kelvin units (K) passing from erg/cm^3 to $K/f.u.$ with subsequent division of the number of magnetic ions of the unit formula.

Fig. 4 b) determines the dependence of K_1 at undoped garnet on the size of the MNPs. This figure was obtained on the basis of experimental results published in [40,65,66]. The following conclusions can be drawn:

1) Within this article, we discuss the magnetic properties of MNPs with a size of (20 - 35) nm. It is obvious that for them the constant of the magnetic anisotropy is one order of magnitude higher compared to the bulk samples (see Fig.4).

2) We assume that the surface magnetic anisotropy depends on x and T in the same way as in the bulk samples (see Fig. 3 and Fig. 4). The reason for this assumption is that by doping with nonmagnetic ions the magnetic anisotropy is determined only by the Fe^{3+} ions.

The numerical calculations and the discusion for the temperatute of the magnetic phase transition T_C, the saturation magnetization M_S and coercivity H_C as a function of the degree of doping x and the size d of MNPs for the mixed yttrium garnets nanoparticles with structure formula $Y_3[Fe_{2-y}M_y]_a(Fe_{3-z}M_z)_dO_{12}$ as M = (Al, Ga, In, Sc) are given in our previous paper[29]. Based on this analysis, we determined a set of magnetic nanoparticles that satisfy the biocompatibility condition and determine their thermal efficiency (see Table 1 in the Introduction).

First we present the dependence of the SAR values on the external parameters: 1) the amplitude of the alternating magnetic field h_0; 2) its frequency f.

Fig. 5 a) and Fig. 5 b) show the dependence of the SAR parameters on the electromagnetic field: the amplitude h_0 and the frequency f at a fixed size of MNPs suitable for SCMH. The quadratic dependence of the thermal efficiency on h_0 and linear on f has been established. Obviously, it is more advantageous to change the field amplitude at lower frequency values because this leads to higher SAR values. On the other hand, the resonance condition $(2\pi f \times \tau_R = 1)$ must be taken into consideration where τ_R is time for the relaxation for the Neel's relaxation mechanism [14]. At very low frequencies this condition is violated, which leads to a strong reduction in SAR even at high field values. These results are in qualitative coincidence with the experimental results [49,67,68] and are proof of the adequacy of the microscopic model, approximations used by us and the accuracy of the calculations. This is due to the fact that the microscopic theory of SAR constructed by us [42] on the basis of Kubo formalism formally has many similarities with the linear response theory (LRT) describing similar dynamic behaviour of MNP in an alternating electromagnetic field with respect to the dependence of thermal efficiency on the amplitude and the frequency of the external magnetic field (the nature of the elliptic hysteresis curves is similar). However, there is an important difference between these two models connected with magnetization. In LRT, the magnetization used in the calculation of SAR was taken from experiments and assumed to be equal to the magnetization in bulk samples. The latter often leads to overestimated values of SAR. To overcome this problem, a “magnetically dead” layer on the surface of the nanoparticles is usually considered which reduces the magnetization and thus, the calculated SAR values are more realistic. In our model, the magnetization is calculated taking into account the crystal structure, as the deviation of the crystal structure on the

IARJSET ISSN (O) 2393-8021, ISSN (P) 2394-1588

International Advanced Research Journal in Science, Engineering and Technology

Impact Factor 7.105 ⁜ Vol. 9, Issue 2, February 2022

DOI: 10.17148/IARJSET.2022.9219

surface is taken into account by reducing the number of nearest neighbours and changing the constants of the exchange interaction. The exchange interaction constants can be conveniently chosen to correctly describe the magnetization of the nanoparticles and the temperature of the magnetic phase transition.

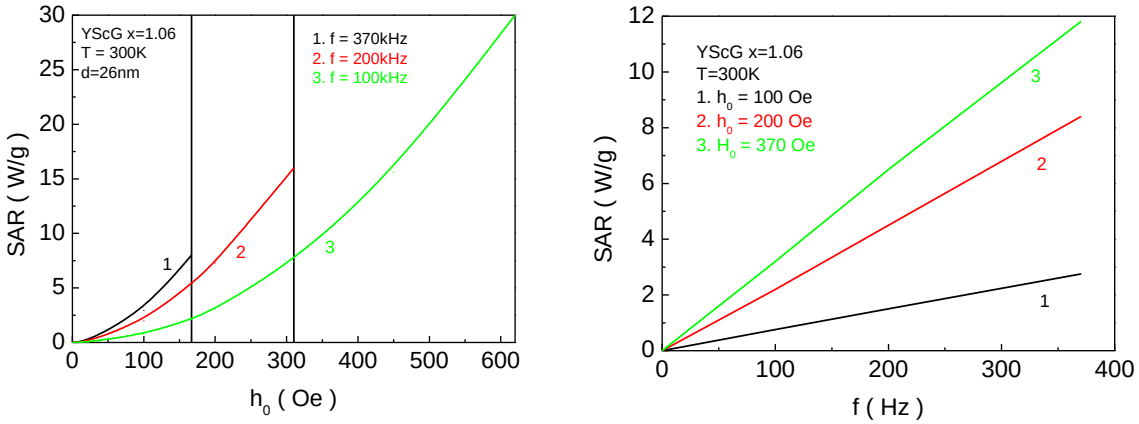

a) b)

Fig. 5 Dependence of SAR on: a) amplitude h_0 for different frequencies 1) f = 370 kHz; 2) f = 200 kHz and 3) f = 100 kHz, the vertical black lines determine the limit of bio tolerance of the human organism to an alternating magnetic field $h_0 * f \leq 6.2 \times 10^7 Oe/s$; b) frequency f for different amplitudes of the alternating field 1) h_0 = 100 Oe; 2) h_0 = 200 Oe and 3) h_0 = 370 Oe for YScG at $T = 300$ K and NP size d = 26 nm.

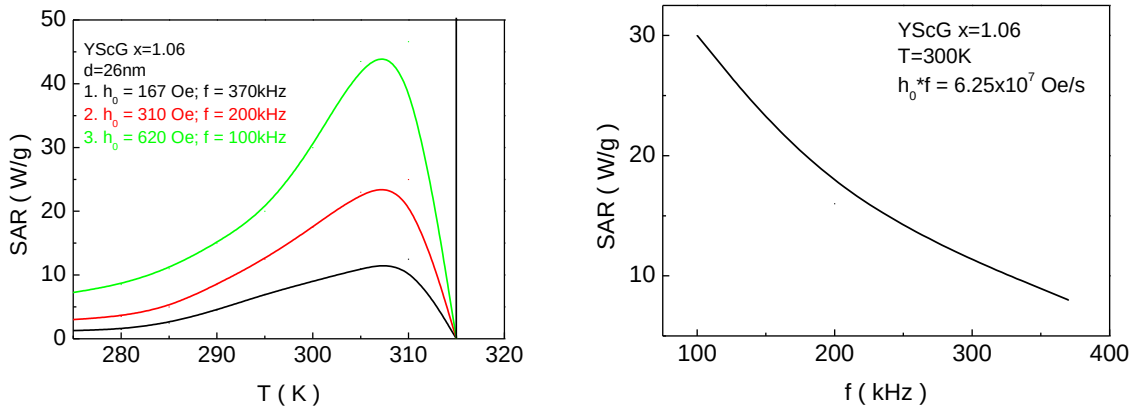

a) b)

Fig. 6. Dependence of SAR on: a) temperature for different values of the amplitude h_0 and the frequency f of the alternating electromagnetic field: 1) h_0 = 167 Oe; f= 370 kHz; 2) h_0 = 310 Oe; f = 200 kHz; 3) h_0 = 620 Oe; f = 100 kHz; (the three curves have been obtained under the condition $h_0 * f = 6.2 \times 10^7 Oe/s$); b) the frequency f (calculations for each frequency are made at such amplitude h_0 of the field, for which the equality $h_0 * f = 6.2 \times 10^7 Oe/s$ is fulfilled) for YScG at $T = 300$ K and size of the NP d = 26 nm.

Fig. 6 a) determines the temperature dependence of the SAR close to the temperature of the magnetic phase transition, but lower than it for three pairs of values for the amplitude and frequency of the external field, which satisfy the biocompatibility condition ($h_0 * f$ factor). For all curves, the SAR peak is observed at the same temperature $T = 308$ K, i.e. it is independent on the field characteristics. It is clear that the temperature dependence of the thermal efficiency in Neel relaxation has a resonant shape and increases sharply near T_N. As the field increases from 167 Oe to 620 Oe, the SAR maximum increases approximately 8 times. This means that there is a possibility of a significant increase in the heating intensity during the procedure and reduction of its duration as well. In the temperature range from 290 K to 308 K, SAR increases although τ_R decreases with increasing of the temperature. This can be qualitatively explained by the type of the expression for the area of the hysteresis curve from [14] and that in this temperature range the magnetization changes slightly with temperature. In the range from 308 K to 315 K a sharp drop in thermal efficiency observes. This

IARJSET ISSN (O) 2393-8021, ISSN (P) 2394-1588

International Advanced Research Journal in Science, Engineering and Technology

Impact Factor 7.105 ⁜ Vol. 9, Issue 2, February 2022

DOI: 10.17148/IARJSET.2022.9219

is a consequence of the sharp drop in the magnetization near the phase transition temperature. This behaviour is in accordance with [69].

Fig. 6 b) presents the dependence of SAR on frequency as for each f the calculation is performed for such amplitude h_0 of the field for which the condition for safe influence of the alternating electromagnetic field is fulfilled, i.e. $h_0 * f = 6.2 \times 10^7 Oe/s$. Numerical calculations clearly show the sensitivity of the thermal efficiency of mixed garnet nanoparticles when changing the parameters of the alternating magnetic field (AMF). The calculations were made in compliance with the resonance requirement $(2\pi f \times \tau_R = 1)$. This fact shows that for frequencies in the range from 100 Hz to 200 Hz, for mixed garnet nanoparticles a good thermal efficiency should be achieved. This will also reduce the time during which the patient is exposed to high-frequency electromagnetic fields.

As noted above, the degree of doping significantly changes the magnetic characteristics of mixed garnets: with increasing of doping with nonmagnetic ions, the value of single-ion anisotropy and magnetic inter-exchange interaction decrease. In Fig. 7 is presented the dependence of SAR on $|J_{ab}|$at $T = 300$ K and $h_0 = 200$ Oe; for different values of the frequency of the alternating electromagnetic field. It is clear that for d=32nm when $|J_{ab}|$ increases the value of SAR decreases (Fig.7 a)). Vice versa for the MNP with a size d=22.5nm the thermal efficiency increases with $|J_{ab}|$ increases (Fig.7 b)). This behaviour is fully expected due to the following qualitative considerations: a/ Fig. 3 a) and Fig. 3 b) show that as the degree of doping increases, the value of the single-ion anisotropy decreases and $|J_{ab}|$ decreases (Fig. 4). b/ On the other hand the relaxation time depends exponentially on the magnetic anisotropy [52] of a MNP and through the resonant term in the expression of thermal efficiency in linear response theory [14] affects the values of SAR.

1/According to (Fig. 8) for d=32nm with increasing the degree of dopping x thermal efficiency increases (see the green vertical line) t.e when $|J_{ab}|$ decreases. For a large values of size of NPs (d=32nm) when the anisotropy increases the spins are practically blocked and only a weak precession near the equilibrium position may be observed. This means that with decreasing of K_1 and the magnetization moves more and more easily between the stable energy states (the spins unblocked) and the the area of the hysteresis increases and the thermal losses grow t.e the value of SAR increases. This situation explains the fact that with decreasing the absolute value of inter-super-exchange interaction $|J_{ad}|$ SAR grows (Fig. 7a).

2/According to (Fig. 8) for d=22.5nm with increasing the degree of dopping x thermal efficiency decreases (see the black vertical line) t.e. when $|J_{ab}|$ decreases. For a small values of size of NPs (d=22,5nm) with decreasing of K_1 the magnetization moves easily between the stable energy states (the $K_1V < k_BT$, where V is the volume of the nanoparticle is fulfield) stimulated by thermal fluctuations. This means that the area of the hysteresis loops get smaller and smaller. Then the thermal losses reduce when magnetic anisotropy decreases. This situation explains the fact with decreasing the absolute value of inter-super-exchange interaction $|J_{ad}|$ SAR rate down (Fig. 7b).

This behaviour is important for the effectiveness of SCMH because when we vary the degree of doping and the size of the MNP, we fit the phase transition temperature into the bio-acceptable range (315 K). It is clear that in the range of concentrations for which a bio-acceptable phase transition temperature is achieved, the thermal efficiency increases.

IV. CONCLUSION

In this paper we study doped YIG MNPs $Y_3[Fe_{2-y}M_y]_a(Fe_{3-z}M_z)_dO_{12}$ (M = Al, Ga, Sc are nonmagnetic ions) appropriate for SCMH for in vivo and in vitro applications. A microscopic model (modified Heisenberg Hamiltonian) and the Green's function technique are used to investigate the dependence of SAR coefficient on the amplitude and the frequency of the alternating magnetic dield, the temperature, and the magnetic inter-exchange interaction. Using the Tserkovnikov's method the static and dynamic characteristics of the magnetic nanoparticles beyond the random phase approximation (taking into account the correlation functions) are calculated. Analytical expressions for the elementary spin excitations energies and their damping are presented. It was found that: 1/ For d=32nm when $|J_{ab}|$ decreases thermal efficiency increases but for d=22.5nm when $|J_{ab}|$ reduces the vavue of the SAR grows. This behavior is explained on the basis of competition between thermal spin fluctuations (which predominated in little MNPs with low magnetic anisotropy) and precession near the equilibrium position for the practically blocked spins (which is characteristic of big MNPs with high magnetic anisotropy). On the base of methodology proposed for the fisrt time are determinated the inter-sublattice and intra-sublattice magnetic exchange constants for different degrees of doping. This behaviour is important for the effectiveness of SCMH because when we vary the degree of doping and the size of the MNP, we fit the phase transition temperature into the bio-acceptable range (315 K). It is clear that in the range of concentrations for which a bio-acceptable phase transition temperature is a chieved, the thermal efficiency increases.

IARJSET ISSN (O) 2393-8021, ISSN (P) 2394-1588

International Advanced Research Journal in Science, Engineering and Technology

Impact Factor 7.105 ⁜ Vol. 9, Issue 2, February 2022

DOI: 10.17148/IARJSET.2022.9219

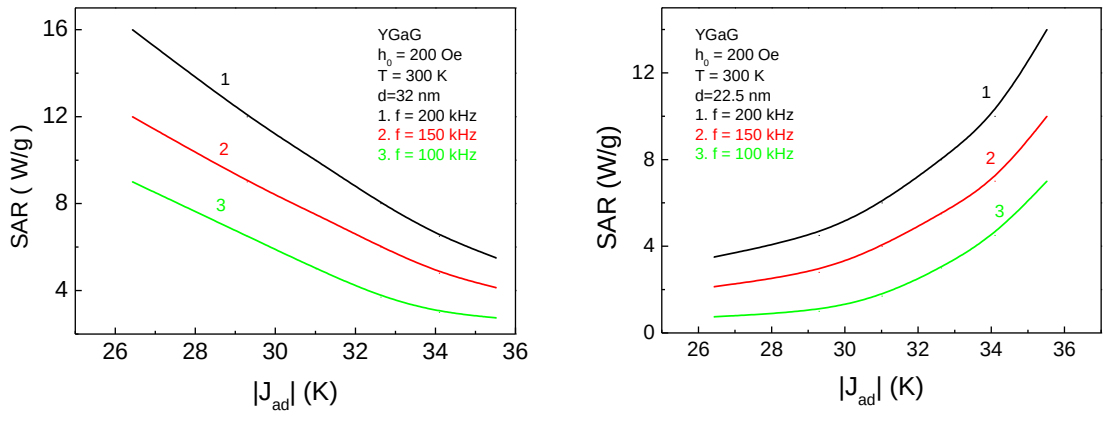

a) b)

Fig. 7 Dependence of SAR on $|J_{ab}|$ at $T = 300$ K and $h_0 = 200$ Oe; for different values of the frequency of the alternating electromagnetic field: 1) f = 200 kHz; 2) f = 150 kHz and 3) f = 100 kHz for sizes of YGaG-MNP a) d=32 nm b) d=22.5nm.

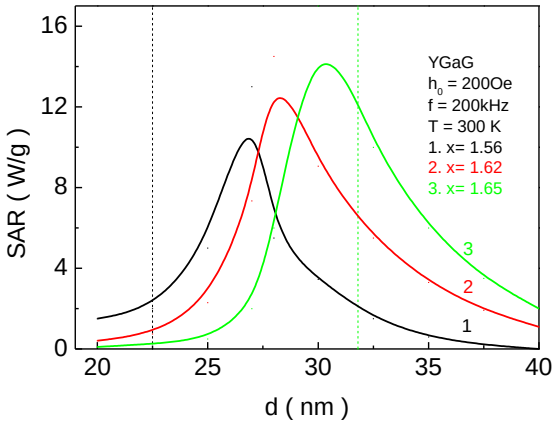

Fig. 8 Dependence of SAR on the size of the YGaG MNPs for the different the degree of doping: 1/ x=1.56; 2/ x=1.62 and 3/ x=1.65 for $T = 300$K and $h_0 = 200$ Oe; f = 200 kHz. The vertical dotted lines determine MNP with fixed sizes: the green one d=32nm and the black – d=22.5nm.

ACKNOWLEDGMENT

One of us (A.T.A) The authors acknowledge support from Center for Research and Desing of the University of Architecture, Civil Enggineering and Geodesy for the financical support (contract number BN-257/22).

Appendix A:

The calculated Green's functions for $Y_3[Fe_{2-y}M_y]_a(Fe_{3-z38}M_z)_dO_{12}$ in the random phase approximation are:

$$G^{aa}_{ij,E} = \frac{i}{\pi}\frac{(E-E^{dd}_{ij})<S^{az}_i>}{(E-E^{aa}_{ij})(E-E^{dd}_{ij})-E^{ad}_{ij}E^{da}_{ij}}\delta_{ij};\quad G^{dd}_{ij,E} = \frac{i}{\pi}\frac{(E-E^{aa}_{ij})<S^{dz}_i>}{(E-E^{aa}_{ij})(E-E^{dd}_{ij})-E^{ad}_{ij}E^{da}_{ij}}\delta_{ij}$$

$$G^{da}_{ij,E} = \frac{i}{\pi}\frac{(E-E^{da}_{ij})<S^{az}_i>}{(E-E^{aa}_{ij})(E-E^{dd}_{ij})-E^{ad}_{ij}E^{da}_{ij}}\delta_{ij};\quad G^{ad}_{ij,E} = \frac{i}{\pi}\frac{(E-E^{ad}_{ij})<S^{dz}_i>}{(E-E^{aa}_{ij})(E-E^{dd}_{ij})-E^{ad}_{ij}E^{da}_{ij}}\delta_{ij}, \qquad (A.1)$$

where:

$$E^{aa}_{ij} = \frac{2}{N}\sum_k J^{aa}_{ik\,eff} < S^{az}_k > \delta_{ij} - 2\sum_k J^{aa}_{ij\,eff} < S^{az}_k > \delta_{ij} - \frac{2}{N}\sum_k J^{ad}_{ik} < S^{dz}_k > -g\mu_B h\delta_{ij};$$

IARJSET ISSN (O) 2393-8021, ISSN (P) 2394-1588

International Advanced Research Journal in Science, Engineering and Technology

Impact Factor 7.105 ⁜ Vol. 9, Issue 2, February 2022

DOI: 10.17148/IARJSET.2022.9219

$E_{ij}^{dd} = \frac{2}{N}\sum_k J_{ik\,eff}^{dd} < S_k^{dz} > \delta_{ij} - 2\sum_k J_{ij\,eff}^{dd} < S_k^{dz} > \delta_{ij} - \frac{2}{N}\sum_k J_{ik}^{da} < S_k^{az} > -g\mu_B h\delta_{ij};$

$E_{ij}^{da} = 2J_{ik}^{da} < S_k^{dz} > \delta_{ij};\ E_{ij}^{ad} = 2J_{ik}^{ad} < S_k^{az} > \delta_{ij},$

with: $J_{ik\,eff}^{aa} = J_{ik}^{aa} + K_i^a\delta_{ij};\ J_{ik\,eff}^{dd} = J_{ik}^{dd} + K_i^d\delta_{ij}.$

Appendix B:

The analytical expressions of the energies ξ_{kl}^{γ} are calculated to:

$$\xi_{ij}^{a} = \frac{1}{< S_i^{az} >}\left\{\frac{2}{N}\sum_k J_{ik\,eff}^{aa}(< S_k^{a-}S_j^{a+} > -2 < S_k^{az}S_j^{az} >) - J_{ij\,eff}^{aa}(< S_i^{a-}S_j^{a+} > - < S_i^{az}S_j^{az} >)\right.$$

$$-\frac{2}{N}\sum_k J_{ik\,eff}^{ad}(< S_k^{d-}S_j^{a+} > -2 < S_k^{dz}S_j^{az} >) - J_{ij\,eff}^{ad}\left(< S_i^{d-}S_j^{a+} > - < S_i^{dz}S_j^{az} >\right)$$

$$\left.-g\mu_B h < S_k^{az} > \delta_{ij}\right\}$$

$$\xi_{ij}^{d} = \frac{1}{< S_i^{dz} >}\left\{\frac{2}{N}\sum_k J_{ik\,eff}^{dd}(< S_k^{d-}S_j^{d+} > -2 < S_k^{dz}S_j^{dz} >) - J_{ij\,eff}^{dd}(< S_i^{d-}S_j^{d+} > - < S_i^{dz}S_j^{dz} >)\right.$$

$$-\frac{2}{N}\sum_k J_{ik\,eff}^{da}(< S_k^{a-}S_j^{d+} > -2 < S_k^{az}S_j^{dz} >) - J_{ij\,eff}^{ad}\left(< S_i^{a-}S_j^{d+} > - < S_i^{az}S_j^{dz} >\right)$$

$$\left.-g\mu_B h < S_k^{dz} > \delta_{ij}\right\} \qquad \text{(B.1)}$$

Appendix C:

The damping for $Y_3\left[Fe_{2-y}M_y\right]_a(Fe_{3-z38}M_z)_dO_{12}$, giving only those terms for which the law on energy conservation is fulfilled:

$$\Gamma_{ij}^{aa} = \frac{4\pi}{N}\sum_l (J_{il}^{aa})^2\,\langle S_l^{az}\rangle\left\{n_l^{aa} * \left[2\langle S_j^{az}\rangle + n_l^{aa} + n_i^{aa}\right] - n_i^{aa}n_l^{aa}\right\}\delta\left(E_l^{aa} + E_j^{aa} - E_i^{aa} - E_l^{aa}\right);$$
$$\Gamma_{ij}^{dd} = \frac{4\pi}{M}\sum_l \left(J_{il}^{dd}\right)^2\,\langle S_l^{dz}\rangle\left\{n_l^{dd} * \left[2\langle S_j^{dz}\rangle + n_l^{dd} + n_i^{dd}\right] - n_i^{dd}n_l^{dd}\right\}\delta\left(E_l^{aa} + E_j^{aa} - E_i^{aa} - E_l^{aa}\right);$$
$$\Gamma_{ij}^{ad} = \frac{4\pi}{N}\sum_l \left(J_{il}^{ad}\right)^2\,n_i^{ad} * n_l^{ad}\,\delta\left(E_i^{ad} - E_l^{ad}\right)\delta_{lj};$$
$$\Gamma_{ij}^{da} = \frac{4\pi}{N}\sum_l \left(J_{il}^{da}\right)^2\,n_i^{da} * n_l^{da}\,\delta\left(E_i^{da} - E_l^{da}\right)\delta_{lj} \qquad \text{(C.1)}$$

where $n_i^{\gamma\eta} = \frac{1}{N}\sum_j \langle S_i^{\gamma-}S_j^{\eta+}\rangle$ and $E_i^{\gamma\eta} = \frac{1}{N}\sum_j E_{ij}^{\gamma\eta}$ for $\gamma, \eta = a, d.$

$$A_1 = E_{ij}^{dd}E_{ij}^{aa} - E_{ij}^{ad}E_{ij}^{da} - \Gamma_{ij}^{aa}\Gamma_{ij}^{dd} - \Gamma_{ij}^{ad}\Gamma_{ij}^{da}; \qquad \text{(C.2)}$$

$$A_2 = E_{ij}^{dd} + E_{ij}^{aa}; \qquad \text{(C.3)}$$

$$A_3 = E_{ij}^{dd}\Gamma_{ij}^{aa} + E_{ij}^{aa}\Gamma_{ij}^{dd} + E_{ij}^{da}\Gamma_{ij}^{ad} + E_{ij}^{ad}\gamma_{ij}\Gamma_{ij}^{da}; \qquad \text{(C.4)}$$

$$\gamma' = \Gamma_{ij}^{aa} + \Gamma_{ij}^{dd}. \qquad \text{(C.5)}$$

IARJSET ISSN (O) 2393-8021, ISSN (P) 2394-1588

International Advanced Research Journal in Science, Engineering and Technology

Impact Factor 7.105 ⁜ Vol. 9, Issue 2, February 2022

DOI: 10.17148/IARJSET.2022.9219

REFERENCES

[1] S. Nagarajan, Z. Yong, Recent Paremts Biomed. Eng. 1 (2008) 34.
[2] O. Bruns, H. Ittrich, K. Peldschus, M. Kaul, U. Tromsdorf, J. Lauterwasser, M. Nikovich, B. Mollwitz, M. Merkel, N. Bigall, Nat. Nanotechnol. 4, 193 (2009)
[3] Q. Pankhurst, N. Thanh, S. Jones, J. Dabson, J. Phys. D: Appl. Phys. 42, 224001 (2009)
[4] A. Gupta, M. Gupta, Biomaterials 26, 3995 (2005)
[5] S. Mornet, S. Vasseur, F. Duguet, J. Mater. Chem. 14, 2161 (2004)
[6] A. Ito, H. Honda and T. Kobayashi, Cancer Immunol. Immunother. 55 (2006) 320.
[7] Z. Shateradadi, G. Nabiyouni, M. Soleymani, Prog. Biophys. Mol. Biol. 133 (2018) 9.
[8] S. Dutz, R. Hergt, J. Murbe, R. Muller, M. Zeisberger, W. Andra, J. Topfer, M. Bellemann, J. Magn. Magn.Mater. 308 (2007) 305.
[9] R. A. K. Pradhan, R. Bah, R. B. Konda, R. Mundle, H. Mustafa, O. Bamiduro, R. R. Rakhimov, J. Appl. Phys. 103 (2008) 07F704.
[10] R. Y. Hong, J. H. Li, J. M. Qu, L. L. Chen, H. Z. Li, Chem. Eng. J. 150 (2009) 572.
[11] O. R. Rajagopal, J. Mona, S. N. Kale, T. Bala, R. Pasricha, P. Poddar, M. Sastry, B. L. V. Prasad, D. C. Kundaliya, S. B. Ogale, Appl. Phys. Lett. 89 (2006) 023107.
[12] S. Jadhav, D. Nikam, V. M. Khot, N. Thorat, M. Phadatare, R. S. Ningthoujam, A. B. Salunkhe, S. H. Pawar, New J. Chem. 37 (2017) 3121.
[13] Z. Li, M. Kawashita, N. Araki, M. Mitsumori, M. Hiraoka, M. Doi, Mater. Sci. Eng.-Mater. Biol. Appl. 30 (2010) 990.
[14] J. Carrey, B. Mehdaoui and M. Respaud, J. Appl. Phys. **2011**, 109, 083921.
[15] Z. Li, M. Kawashita, N. Araki, M. Mitsumori, M. Hiraoka, M. Doi, Mater. Sci. Eng.-Mater. Biol. Appl. 30 (2010) 990.
[16] R. E. Rosensweig, J. Magn. Magn. Mater. 252 (2002) 370.
[17]W. Brown, Phys. Rev. B 130 (1963) 1677.
[18] B. Jeyadevan, J. Chem. Soc. Jpn. 118 (2010) 391.
[19] R. Hergt, W.Andra, C. d'Ambly, I. Hilger, W.Kaiser, U.Richter, H.Schmidt, IEEE Trans. Magn. 34 (1998) 3745.
[20] K. Krishnan, IEEE Trans. Magn. 46 (2010) 2523.
[21] G. Landi, Phys. Rev. B 89 (2014) 014403.
[22] S. Lee, J. Jeong, S. Shin, J. Kim, J. Magn. Magn. Mater. **2004**, 282, 147.
[23] A. T. Apsotolov, I. N. Apostolova, J. M. Wesselinowa, Eur. Phys. J. B **2013**, 86, 483.
[24] R. Arulmurugan, G. Vaidyanathan, S. Sendhilnathan, B. Jeyadevan, J. Magn. Magn. Mater. **2006**, 298, 83.
[25] A. Rashid and S. Manzoor, J. Magn. Magn. Mater. **2016**, 420, 232.
[26] M. Soleymani, M. Edrissi and A. M. Alizadeh, J. Mater. Chem. B **2017**, 5, 4705.
[27] T. Nishimori, Yu. Akiyama, T. Naohara, T. Maehara, H. Hirazawa, Yo. Itagaki and H. Aono, Jour Ceram. Soc. Jpn. 122 (2014) 35.
[28] H. Aono, Jour Ceram. Soc. Jpn. 122 (2014) 237.
[29] A.Apostolov, I.Apostolova and J.Wesselonowa, Phys. Stat. Sol b, ….(2022)
[30] I. Apostolova, A. Apostolov and J. Wesselinowa, J. Magn. Magn. Mater. **2021**, 522, 167504.
[31] Vu Huong, D. Nguyet, N. Duong, T. Loan, S. Soontaranon, L. Anh, Add. Mater. Dev. 5 (2020) 270.
[32] M.A.Gilleo and S.Geller, Phys.Rev. 110 (1958) 73.
[33] B. Ravi, X. Gou, Q. Yan, R. Gambino, S. Sampath and J. Parise, Sur. Coat. Techn. 201 (2007) 7597.
[34] D. Strenzwilk and E. Ardenson, Phys. Rev. 175 (1968) 654.
[35] P. Gornert and C. d'Ambly, Phys. Stat. Sol. (a) 29 (1975) 95.
[36] S. Geller, J. Cape, G. Espinnosa and D. Leslie, Phys. Rev. 148 (1966) 522.
[37] K. Belov and I. Sokolov, Sov.Phys. Usp. 20 (1977) 149.
[38] T. Kim and M. Shima, Jor. All. Phys. 101 (2007) 09M516.
[39] A. Morrish, and K. Haneda, J. Phys. Colloq. 41 (1980) C1-171.
[40] M. Rajendran, S. Deka, P. Joy and A. Bhattacharya, Jour. Mang. Magn. Mater. 301 (2006) 212.
[41] D. Nguyet, N. Duong, T. Satoh, L. Anh and Th. Hien, Jour Alloys Comp. 541 (2012) 18.
[42] J. M. Wesselinowa and I. Apostolova, J. Phys.: Condens. Matter 19 (2007) 216208.
[43] G. Dionne, J. Appl. Phys. 41 (1970) 4847.
[44] P. Roschmann and P. Hansen, Jour. Appl. Phys. 52 (1981) 6257.
[45] J. Korcki, M. Przybylski, U. Gradmann, J. Magn. Magn. Mater. 89 (1990) 325.
[46] S. V. Tyablikov, Methods in the Quantum Theory of Magnetism, Plenum Press, New York (1967).
[47] R. Hergt, W.Andra, C. d'Ambly, I. Hilger, W.Kaiser, U.Richter, H.Schmidt, IEEE Trans. Magn. 34 (1998) 3745.
[48] G. Landi, Phys. Rev. B 89 (2014) 014403.

DOI: 10.17148/IARJSET.2022.9219

[49] E. Vedre, G. Landi, M. Carriao, A. Dummond, J. Gomes, E. Vieira, M. Sousa, A. Drummond, AIP Adv. 2 (2012) 032120.
[50] S. Ruta, R. Chantrell, O. Hovorka, Sci. Rep. 5 (2015) 9090.
[51] L. C. Branquinho, M. S. Carrião, A. S. Costa, N. Zufelato, M. H. Sousa, R. Miotto, R. Ivkov and A. F. Bakuzis, Sci. Rep. 3 (2013) 2887.
[52] E. Verde, G. Landi, J. Gomes, M. Sousa, A. Bakuzis, J. Appl. Phys 111 (2012) 123902.
[53] C. Martinez-Boubeta, K. Simeonidis, A. Makridis, M. Angelakeris, O. Iglesias, P. Guardia, A. Cabot, L. Yedra, S. Estradé, F. Peiró, Z. Saghi, PA. Midgley, I. Conde-Leborán, D. Serantes, D. Baldomir. Sci. Rep. 3 (2013) 1652.
[54] Yu. Tserkovnikov, Theor. Math. Phys. 7 (1971) 250.
[55] R.L.Streever and G.A.Uriano, Phys. Rev.139 (1965) 305.
[56] P. Roschmann, Jour Chem. Sol. 41 (1980) 569.
[57] E. E. Anderson, Phys. Rev. 134 (1964) A1581.
[58] L. Xie, G. Jin, L. He, G. Bauer, J. Backer and K. Xia, Phys. Rev. B 95 (2017) 014423.
[59] R. Philips and L. White, Phys. Rev. Lett. 16 (1966) 650.
[60] A. Clark, B. Desavage and W. Coleman, J. Appl. Phys. 34 (1963) 1296.
[61] S. Mandel, M. Smokotin, A. Petrakovskii and M. Lebed, Phys. Stat. Sol. 30 (1968) K111.
[62] A. Petrakovskii, M. Smokotin and A. Sablina, Fiz. Tver. Tela 9 (1967) 2324.
[63] G .Winkler, Magnetic Garnets, F.Vieweg and Sohn, Braunschweig/Weisbaden (1981).
[64] P. Hansen, Philips Research Reports Suppl. 7 (1970) 1.
[65] R. Sanches, J. Rivas, P. Vaqeiro, M. Lopez-Quintela, D. Caeiro, Jour. Magn. Magn. Mater. 247 (2002) 92.
[66] T. Nguyet, N. Duong, T. Satoh, L. Anh and Th. Hien, Jour. Allows and Comp. 541 (2012) 18.
[67] P. Guardia, R. Corado, L. Lartigie, C. Wilhelm, A. Espinosa, M. Garsia-Hernandes, F. Gazeau, T. Pelligrino, ACS Nano 6 (2012) 3080.
[68] A. Hiromichi, Jour. Chem. Soc. Jpn. 122 (2014) 237.
[69] G. Barrera, P. Allia, and P. Tiderto, Nanoscale 12 (2020) 6360.

